

# Atomic configuration and properties of austenitic steels at finite temperature: The effect of longitudinal spin fluctuations

A. V. Ruban

*Department of Materials Science and Engineering,  
KTH Royal Institute of Technology, SE-100 44 Stockholm, Sweden and  
Materials Center Leoben Forschung GmbH, A-8700 Leoben, Austria*

M. Dehghani

*Materials Center Leoben Forschung GmbH, A-8700 Leoben, Austria*

(Dated: June 6, 2022)

High temperature atomic configurations of fcc Fe-Cr-Ni alloys with alloy composition close to austenitic steel are studied in statistical thermodynamic simulations with effective interactions obtained in *ab initio* calculations. The latter are done taking longitudinal spin fluctuations (LSF) into consideration within a quasiclassical phenomenological model. It is demonstrated that magnetic state affects greatly the alloy properties and in particular, it is shown that the LSF substantially modify the bonding and interatomic interactions of fcc Fe-Cr-Ni alloys even at ambient conditions. The calculated atomic short-range order (SRO) is in reasonable agreement with existing experimental data for  $\text{Fe}_{0.56}\text{Cr}_{0.21}\text{Ni}_{0.23}$ , which has strong preference for the (001) type ordering between Ni and Cr atoms. A similar ordering tendency is found for the  $\text{Fe}_{0.75}\text{Cr}_{0.17}\text{Ni}_{0.08}$  alloy composition, which approximately corresponds to the widely used 304 and 316 austenitic steel grades.

## I. INTRODUCTION

Austenitic steels based on Fe-Cr-Ni system are in extensive use in different domestic and industrial applications due to their excellent corrosion resistant and mechanical properties. They usually consist of more than three elements added on a purpose or accidentally, however, Cr and Ni are the usual alloying elements: Cr provides the corrosion resistance, and its content is usually in between 15–25 at. %, while Ni stabilizes the fcc structure, and its content is as a rule within 5–15 at.% (can be up to 35 at.% in some special grades). Although these alloys have been for decades under development and investigation, accurate description of their finite temperature properties at the atomic and electronic structure levels is still a challenging task.

One of the main obstacles in getting accurate *ab initio* picture of fcc Fe-Cr-Ni alloys is their non-trivial magnetism. The magnetic phase diagram of  $\text{Fe}_{80-x}\text{Ni}_x\text{Cr}_{20}$  ( $10 \leq x \leq 30$ ) alloys have been determined in Ref. 1. At low temperatures, one can find antiferromagnetic, spin-glass, ferromagnetic and a mixture of ferromagnetic and spin glass states for a certain range of compositions. In particular, the antiferromagnetic state is the low temperature magnetic state with the Neel temperature of about 20–40 K if concentration of Ni is within 5–15 at. %. This means that in practice austenitic steels are in paramagnetic state at ambient conditions.

The problem is that this paramagnetic state is a highly non-trivial phenomenon, which is extremely difficult to model accurately on the first-principles level since a static disordered local moment model breaks down due to disappearance of the local magnetic moments on Cr and Ni atoms in the density functional theory (DFT) calculations. At the same time, their magnitude deviates substantially from zero due to longitudinal spin fluctua-

tions on short time scales, producing a significant effect upon all the properties of steels. In principle, such magnetic excitations can be accounted for using advanced *ab initio* methods like, for instance, dynamical mean-field theory.<sup>2</sup> However, their applications to steels, which are multicomponent random alloys, is too cumbersome.

In this paper, we therefore use a simplified formalism for the LSF developed in Ref. 3 and 4. It is a classical high temperature limit of the spin-fluctuation theory<sup>5,6</sup> where the contribution due to thermally induced spin fluctuations are considered within a phenomenological model based on a classical magnetic Hamiltonian. Although it breaks down at low temperatures where quantum effects are important, it provides a reasonable account of the LSF at elevated temperatures.<sup>4</sup>

Using this model of the LSF, we consider properties of Fe-Cr-Ni alloys and, in particular, atomic ordering at elevated temperatures. The experimental information on the atomic short range order (SRO) in austenitic steels is scarce. A quite detailed investigation of the atomic SRO in fcc  $\text{Fe}_{56}\text{Cr}_{21}\text{Ni}_{23}$  was done by Cenedese *et al.*<sup>7</sup> by thermal neutron diffuse scattering from single crystals. The atomic SRO has been also measured in alloys with similar compositions,  $\text{Fe}_{82-x}\text{Cr}_{18}\text{Ni}_x$  ( $x = 15, 20$ , and 25 wt.%) by Braude *et al.* using x-ray diffuse scattering technique.<sup>8</sup> However, some results of this investigation are contradictory as is discussed below.

Recently, the phase stability of ternary fcc and bcc Fe-Cr-Ni alloys has been investigated in Ref. 9 using a combination of DFT, cluster expansion (CE), and magnetic cluster expansion (MCE) techniques. These authors have found good agreement of different calculated properties with experimental data, including results for the atomic SRO in  $\text{Fe}_{56}\text{Cr}_{21}\text{Ni}_{23}$  alloy as stated by the authors. At the same time, the results presented in Table VII of Ref. 9 show some obvious problems for the calculated atomic

SRO in this alloy. Namely, the calculated atomic SRO is too strong compared with the experimental data,<sup>7</sup> especially taking into consideration the fact that calculations are for 1300 K, while in the experiment, the samples were annealed first for 1 hour at 1273 K and then for 10 hours at 773 K. Of course, it might well be that 10 hours is not enough to fully equilibrate this alloy at 773 K, nevertheless a substantial rearrangement can be expected on a local scale of at least several interatomic distances. In fact, the authors of Ref. 9 find ordering transition at 1550 K for Fe<sub>50</sub>Cr<sub>25</sub>Ni<sub>25</sub>. At this temperature the diffusion is very fast, and had such a high-temperature transition really existed, it or the corresponding ordered phase would be definitely seen or detected in different kind of experiments.

This means that there is a problem with the existing theoretical description of the atomic SRO in austenitic steels. To solve it is one of the aims of the present investigation. Another aim is to demonstrate the role of the LSF in austenitic steels at finite temperatures. For that purpose, we consider here two alloy: Fe<sub>75</sub>Cr<sub>17</sub>Ni<sub>8</sub> alloy, whose composition is close to the widely used 304 and 316 steel grades, and Fe<sub>56</sub>Cr<sub>21</sub>Ni<sub>23</sub>, whose atomic SRO has been obtained experimentally<sup>7</sup> and just recently calculated using *ab initio* theory.<sup>9</sup> We also outline a technique for calculating chemical and magnetic exchange interactions within the exact muffin-tin orbital (EMTO) method.<sup>10,11</sup>

## II. FIRST-PRINCIPLES METHODOLOGY

Electronic structure calculations of random fcc Fe-Cr-Ni alloys have been done using the coherent potential approximation (CPA)<sup>12</sup> and locally self-consistent Green's function (LSGF) technique,<sup>13</sup> which accurately accounts for the local environment effects in random alloys. Both these techniques have been used within the EMTO method<sup>10,11</sup> referenced here as EMTO-CPA<sup>14</sup> and ELSGF<sup>15</sup>, respectively. The EMTO-CPA calculations have been done by the Lyngby version of the Green's function EMTO code,<sup>16</sup> where the screened Coulomb interactions in the single-site DFT-CPA approximation<sup>17</sup> and screened generalized perturbation method (SGPM)<sup>18–20</sup> are implemented (See Appendix A).

In particular, the contributions of the screened Coulomb interactions in the DFT-CPA to the one-electron potential of alloy components,  $V_{\text{scr}}^i$ , and to the total energy,  $E_{\text{scr}}$ , are:<sup>17</sup>

$$V_{\text{scr}}^i = -e^2 \alpha_i^0 \frac{\bar{q}_i}{S}$$

$$E_{\text{scr}} = \sum_i c_i E_{\text{scr}}^i; \quad E_{\text{scr}}^i = -e^2 \frac{1}{2} \alpha_i^0 \beta_{\text{scr}} \frac{\bar{q}_i^2}{S}. \quad (1)$$

where  $\bar{q}_i$  and  $\alpha_i^0$  are the net charge of the atomic sphere of the  $i$ th alloy component in the single-site CPA calcu-

lations and its on-site screening constant, which are different for different alloy components in multicomponent alloys,  $S$  the Wigner-Seitz radius,  $\beta_{\text{scr}}$  the average on-site screening constants, which accounts for the electrostatic multipole moment energy contribution due to inhomogeneous local environment of different sites in random alloy.

The self-consistent electronic structure calculations have been done within the local density approximation using Perdew and Wang functional,<sup>21</sup> while the total energy have been calculated using the full charged density technique<sup>11</sup> in the PBE generalized gradient approximation.<sup>22</sup> In the Brillouin zone integration, a  $32 \times 32 \times 32$  Monkhorst-Pack grid have been used.<sup>23</sup> All the calculations have been done with  $l_{\text{max}} = 3$  for partial waves and the electronic core states were recalculated at every iteration during the self-consistent calculations for valence electrons.

The on-site and inter-site screening constants needed in the EMTO-CPA and SGPM calculations were obtained for Fe<sub>75</sub>Cr<sub>17</sub>Ni<sub>8</sub> and Fe<sub>50</sub>Cr<sub>25</sub>Ni<sub>25</sub> random alloys in a 864-atom supercell ( $6 \times 6 \times 6$  translations of the fcc 4-atom cubic unit cell) ELSGF calculations. After the configurational optimization, the first six Warren-Cowley SRO parameters of the supercells were less than 0.002 (in absolute value) and next 2, for the 7th and 8th coordination shells, less than 0.015 for all three pairs of the alloy components. The calculations were done in the disordered local moment state<sup>24,25</sup> as is implemented in the ELSGF code<sup>15</sup> with the LSF at 800 K (see the next section). The local interaction zone (LIZ) has contained the first two coordination shells of the central site (of the LIZ).

The on-site screening constants have been determined as

$$\alpha_i^0 = \frac{S \langle V_i^{\text{Mad}} \rangle}{e^2 \langle q_i \rangle}, \quad (2)$$

where  $\langle q_i \rangle$  and  $\langle V_i^{\text{Mad}} \rangle$  are the conditional average of the net charges,  $q_i$ , and the Madelung potentials,  $V_i^{\text{Mad}}$  of the  $i$ -th component in the supercell. The calculated on-site screening constants,  $\alpha_i^0$ , vary very little with alloy composition, lattice constant, and temperature due to thermal electronic and magnetic excitations due to the LSF. They are approximately equal to 0.725, 0.777, and 0.823 for Fe, Cr, and Ni, respectively, while  $\beta_{\text{scr}}$  is about 1.14. These values of the screening constants have been used in all the DFT-CPA calculations.

The intersite screening constants,  $\alpha_p^{ij}$ , needed in the calculations of the electrostatic contribution,  $V_p^{ij-\text{scr}}$  to the SGPM potential at the  $p$ th coordination shell for the  $i$ - $j$  pair of alloy components:

$$V_p^{ij-\text{scr}} = e^2 \alpha_p^{ij} \frac{\bar{q}_{ij}^2}{S}, \quad (3)$$

where  $\bar{q}_{ij} = \bar{q}_i - \bar{q}_j$ . Screening constants  $\alpha_p^{ij}$  have been obtained in the supercell ELSGF calculations random alloy

from the screening charge by exchanging the corresponding alloy components ( $i$  and  $j$  in some specific sites having random local environment on average) as is described in Ref. 17.

### III. LONGITUDINAL SPIN FLUCTUATIONS IN Fe-Cr-Ni ALLOYS

The description of the paramagnetic state in fcc alloys in DFT calculations at ambient conditions requires an additional modeling, which takes into consideration thermally induced longitudinal spin fluctuations.<sup>3,4,26–29</sup> Here, we follow the formalism developed in Refs. 3 and 4. The main idea is to consider the LSF as an entropic effect within a static one-electron consideration. In this case, the magnitude of the local magnetic moment induced by the entropy can be obtained, to a first approximation, from the longitudinal spin fluctuation energy in the corresponding statistical thermodynamic simulations.

The longitudinal spin fluctuation energy is the energy of embedding an impurity having a given magnetic moment  $m_i$  into the DLM effective medium with a certain choice of the average local magnetic moments of alloy components.<sup>3</sup> Since, the average local magnetic moment at a given temperature is not known in advance, the statistical simulations have to be done in a self-consistent way.

Obviously, this is an extremely time consuming scheme in the case of multicomponent alloys. However, it can be greatly simplified by using an approximate expression for the entropy of longitudinal spin fluctuations:<sup>4</sup>

$$S_i^{\text{lsf}} = 3 \ln m_i, \quad (4)$$

which is valid in the classical high-temperature limit for the quadratic form of the LSF energy. Although the later is approximately true only for Ni and Cr, while for Fe there is a non zero local magnetic moment for equilibrium lattice constants of austenitic steels, we have used this expression for Fe too in order to keep continuous description of the magnetic energy for small lattice constants.

In Fig. 1, the longitudinal spin fluctuation energy for Fe, Cr, and Ni in  $\text{Fe}_{75}\text{Cr}_{17}\text{Ni}_{08}$  in the DLM effective medium due to the LSF is shown. In these calculations, the local magnetic moment of one of the components have been changed while all the other were kept fixed to the following magnitudes:  $1.69 \mu_B$  for Fe,  $0.82 \mu_B$  for Cr, and  $0.38 \mu_B$  for Ni, which approximately corresponds to their local magnetic moments at 300 K obtained using Eq. (4) in the self-consistent calculations. One can see, that the LSF energy curves for Ni and Cr resemble parabola. In the case of Fe, the LSF energy has minimum at  $\approx 1.4 \mu_B$ . Thus, at least a fourth order polynomial is needed to get a qualitative behavior of the LSF energy in the latter case.

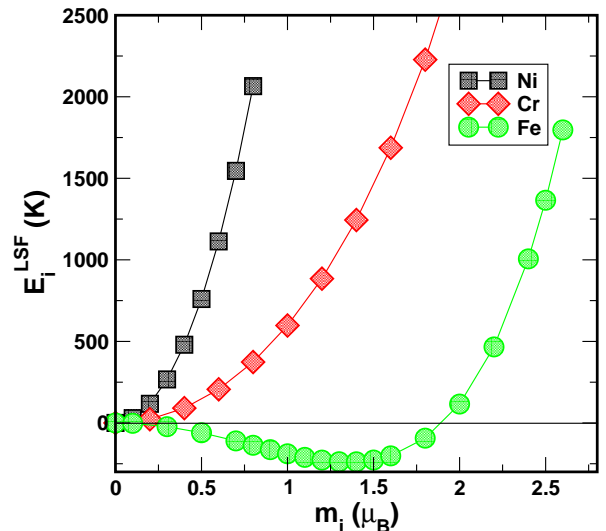


FIG. 1. (Color online) Longitudinal spin fluctuation energies of alloy components in  $\text{Fe}_{75}\text{Cr}_{17}\text{Ni}_{08}$  in the DLM state obtained for the Fe, Cr, and Ni local magnetic moments 1.69, 0.82, and  $0.38 \mu_B$ , respectively.

However, this approximate scheme works reasonably well even for the LSF induced magnetic moment of Fe. In Fig. 2, the local magnetic moments of Ni, Cr, and Fe are shown as function of temperature, which have been obtained in the single-site mean-field approximation from the LSF energies,  $E_i^{\text{LSF}}$ , presented in Fig. 1 as:

$$m_i = 1/Z_i \int E_i^{\text{LSF}}(m) m^3 dm, \quad (5)$$

where  $Z_i$  is the partial statistical sum for alloy component  $i$ :

$$Z_i = \int E_i^{\text{LSF}}(m) m^2 dm, \quad (6)$$

It can be substantially simplified without losing much accuracy (which is not on the demand in semiquantitative modeling) by just calculating the energy of the DLM state with varying magnitude of the local magnetic moment of one of the alloy components while keeping  $m$  of the others fixed to the one which corresponds to the chosen temperature. For instance, using (4) one finds that the local magnetic moments in  $\text{Fe}_{75}\text{Cr}_{17}\text{Ni}_{08}$  at 300 K are 1.69, 0.82, and  $0.38 \mu_B$  for Fe, Cr, and Ni, respectively, while they are 1.52, 0.77, and  $0.35 \mu_B$  if (6) is used with the corresponding spin-fluctuation energies. As one can see, even for Fe, Eq. (4) produces quite reasonable results only slightly overestimating local magnetic moment. Let us note that without LSF the local magnetic moment of Fe is about  $1.4 \mu_B$  while Cr and Ni becomes non-spin polarised.

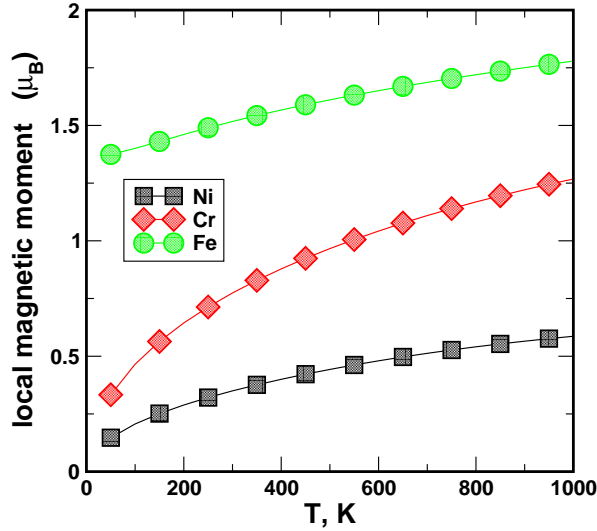


FIG. 2. (Color online) Local magnetic moments of alloy components in  $\text{Fe}_{0.75}\text{Cr}_{0.17}\text{Ni}_{0.08}$  due to LSF obtained from the LSF energies presented in Fig. 1 as a function of temperature.

#### IV. LATTICE PARAMETER AND ELASTIC CONSTANTS OF $\text{Fe}_{75}\text{Cr}_{17}\text{Ni}_{08}$ AT AMBIENT CONDITIONS

The importance of the LSF in austenitic steels even at room temperature can be seen in the first-principles calculations of the lattice constant and bulk modulus of  $\text{Fe}_{75}\text{Cr}_{17}\text{Ni}_{08}$  alloy. In Fig. 3, we show the total energies (up to an arbitrary constant) of random  $\text{Fe}_{75}\text{Cr}_{17}\text{Ni}_{08}$  alloy obtained in the EMT-CPA calculations in the DLM paramagnetic state with and without LSF. In the DLM calculations, the magnetic entropy of Fe has been accounted for using the entropy of the ideal paramagnetic gas ( $S_{mag}^{\text{IP}} = \ln(m_{Fe} + 1)$ ). The one-electron thermal excitations have been included using Fermi-Dirac distribution function.<sup>30</sup>

If LSF are not included, the free energy curve exhibits quite irregular behaviour around Wigner-Seitz (WS) radius of 2.6 a.u. (or lattice constant about 3.52 Å), which can be traced down to the abrupt change of the magnitude of magnetic moment of Fe, which is clearly seen in Fig. 4. The equilibrium WS sphere radii (without phonon contribution) is 2.618 a.u. and bulk modulus is about 210 GPa, which is too large compared to the room temperature bulk modulus of austenitic steels with similar composition, which is usually in the range of 140-170 GPa.<sup>31</sup>

The inclusion of the LSF, apart from smoothing the total energy curve, leads to the increase of the equilibrium WS radius to 2.623 a.u. or lattice constant of 3.55 Å and to a substantial decrease of the bulk modulus: 161 GPa. In the Debye-Grüneisen model, the room temperature lattice constant then comes out to be 3.57 Å and bulk modulus 155 GPa, which are in reasonable agreement with experimental data.<sup>31</sup> The calculated room temper-

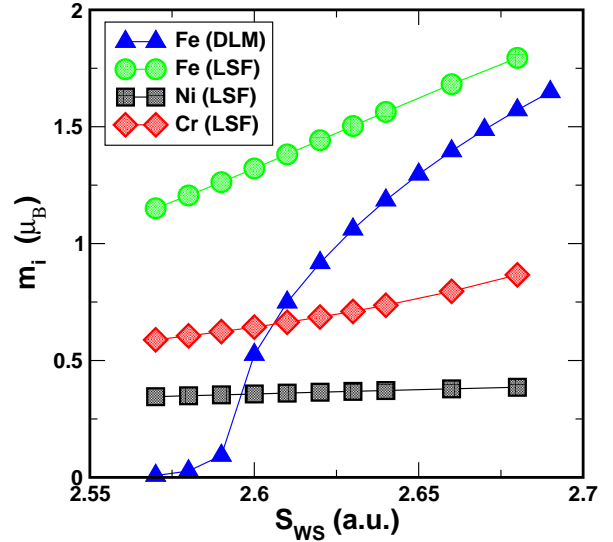
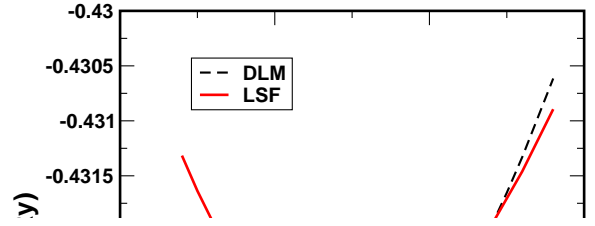


FIG. 4. (Color online) Local magnetic moments of Fe, Cr, and Ni in  $\text{Fe}_{75}\text{Cr}_{17}\text{Ni}_{08}$  in the DLM calculations with and without LSF.

ature shear elastic constants,  $c'$  and  $c_{44}$ : 35 and 138 GPa, respectively, are also in good agreement with the existing experimental data: 38 and 121 GPa.<sup>31</sup>

#### V. EFFECTIVE INTERACTIONS

Finite temperature atomic configuration of  $\text{Fe}_{75}\text{Cr}_{17}\text{Ni}_{08}$  and  $\text{Fe}_{56}\text{Cr}_{21}\text{Ni}_{23}$  has been obtained in Monte Carlo simulations using the following configurational Hamiltonian:

$$H = \frac{1}{2} \sum_p \sum_{\alpha, \beta \neq \delta} V_p^{(2)-\alpha\beta[\delta]} \sum_{ij \in p} \delta c_i^\alpha \delta c_j^\beta + \quad (7)$$

$$\frac{1}{3} \sum_t \sum_{\alpha, \beta, \gamma \neq \delta} V_t^{(3)-\alpha\beta\gamma[\delta]} \sum_{i,j,k} \delta c_i^\alpha \delta c_j^\beta \delta c_k^\gamma + h.o.t..$$

Here, the summation is performed over alloy different type of clusters ( $p$  and  $t$  stands for indexes of the pairs and triangles), alloy components (designated by Greek letters) and lattice sites ( $i$ ,  $j$ , and  $k$ );  $V_p^{(2)-\alpha\beta[\delta]}$  and  $V_t^{(3)-\alpha\beta\gamma[\delta]}$  are the pair- and three-site effective interactions, which have been determined using the SGPM implemented in the Lyngby version of the EMTO-CPA code (see Appendix for details), and  $\delta c_i^\alpha = c_i^\alpha - c^\alpha$  is the concentration fluctuation of the  $\alpha$  component from its average concentration in alloy,  $c^\alpha$  at site  $i$ .

The contribution from pair interactions in (7) can be reduced to a quasibinary form:

$$H^{(2)} = -\frac{1}{2} \sum_p \sum_{\alpha \neq \beta} \tilde{V}_p^{(2)-\alpha\beta} \sum_{ij \in p} \delta c_i^\alpha \delta c_j^\beta, \quad (8)$$

where  $\tilde{V}_p^{(2)-\alpha\beta}$  are the usual binary effective interactions describing the mutual ordering of  $\alpha$  and  $\beta$  atoms and connected with the multipoint effective pair interactions,  $V_p^{(2)-\alpha\beta[\delta]}$  as<sup>32,33</sup>

$$V_p^{(2)-\alpha\beta[\delta]} = \frac{1}{2} \left[ \tilde{V}_p^{(2)-\alpha\delta} + \tilde{V}_p^{(2)-\beta\delta} - \tilde{V}_p^{(2)-\alpha\beta} \right]. \quad (9)$$

The advantage of such a quasibinary representation is its direct connection to the Hamiltonians and interactions of the binary systems of the components composing the multicomponent one. Unfortunately, the contribution from multisite interactions cannot be reduced to a similar quasibinary form due to the presence of additional indexes of alloy components.

In first-principles calculations, the interactions entering Eqs. (7) and (8) have been obtained using a DLM six component model of the three-component alloys: two components with the opposite orientation of magnetic moment for each alloy component. The chemical interactions have been obtained in the magnetic-moment averaged form for each alloy component in the DLM-CPA calculations. The corresponding expressions for the interactions in the EMTO-CPA method are given in Appendix A.

The effective interactions of the above Hamiltonian are not only concentration dependent, but they also depend on the temperature due to the temperature dependence of the equilibrium volume of the alloy, its magnetic state, and the local magnetic moments of its components in the DLM-LSF state. As is demonstrated below such a temperature dependence should be taking into consideration in atomistic modeling at high temperatures.

In Fig. 5, the quasibinary effective pair interactions,  $\tilde{V}_p^{(2)-\alpha\beta}$ , in Fe<sub>75</sub>Cr<sub>17</sub>Ni<sub>8</sub> and Fe<sub>56</sub>Cr<sub>21</sub>Ni<sub>23</sub> of Hamiltonian (8) are shown. They have been obtained for the high temperature (800–1000K) lattice constant of 3.615 Å. Two sets of interactions have been obtained in the DLM-LSF state at 800 K, while one set of interactions, for Fe<sub>56</sub>Cr<sub>21</sub>Ni<sub>23</sub> alloy was calculated in the DLM calculations without LSF. In this case, there is no magnetic moment on Ni and Cr atoms. As one can see, the LSF produce quite substantial effect in the case of Fe-Ni and Fe-Cr effective interactions, although it is not that pronounced in the case of Ni-Cr interactions. At the same time, the concentration dependence seems to be quite moderate, within the range of the accuracy of the SGPM calculations.

The dependence of the effective interactions on the lattice constant is in fact quite strong (not shown in the figure). For instance, the nearest-neighbor effective interactions obtained in the DLM state for the theoretical 0 K lattice constant, 3.55 Å, are 5.89, -0.62, and 10.05 mRy for Fe-Cr, Fe-Ni and Fe-Cr pairs, respectively, which are quite different from those for the high temperature lattice constant of 3.615 Å: 3.96, 0.30, and 8.24 mRy. Obviously, the external and internal parameters cannot be disregarded in finding theoretical atomic configuration of austenitic steels at finite temperatures.

Effective interactions presented in Fig. 5 look qualitatively similar for all the pairs: the strongest interaction of the ordering type at the first coordination shell following the next strongest interaction with the opposite sign at the second coordination shell. However, as we will see below, there cannot be mutual ordering of all the pairs due to the fact that the pairs with the strongest ordering energies, specifically NiCr at the first coordination shell, will be ordering first.

Let us note that the strong ordering interaction of Ni and Cr atoms at the first coordination shell is almost entirely due to the screened Coulomb interaction, which is of an order of 8–9 mRy, while the one-electron contribution is only about 0.2–0.5 mRy. In the case of Fe-Ni and Fe-Cr pairs, the nearest neighbor screened Coulomb interaction is relatively small, about 1 and 2 mRy, respectively. This is an expected result, since the screened Coulomb interactions are proportional to the charge transfer between the corresponding alloy components, which is in its turn determined mostly by their mutual size difference. The latter is obviously the largest for Ni and Cr, while it is relatively small for Fe-Cr and Fe-Ni pairs.

The size difference of alloy components leads to the appearance of local lattice relaxations, which can be accounted for in the configurational Hamiltonian by the so-called strain-induced interactions. Unfortunately, it is impossible to calculate accurately these interactions in ternary Fe-Cr-Ni alloys, especially at high temperatures in the paramagnetic state with LSF. Therefore in this work, we use a simple qualitative model. First of all, we disregard the strain induced interactions for Fe-

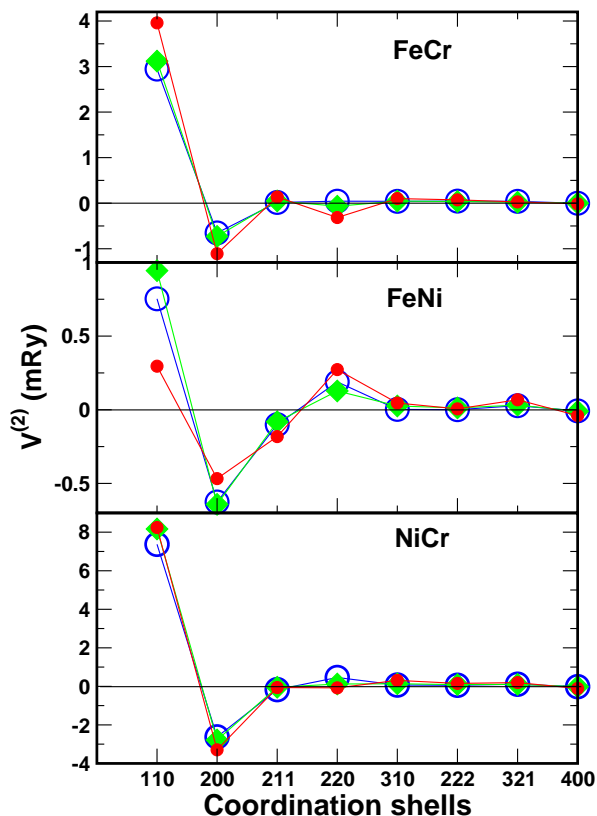


FIG. 5. (Color online) Quasibinary effective pair interactions in  $\text{Fe}_{75}\text{Cr}_{17}\text{Ni}_{08}$  (open circles) and  $\text{Fe}_{56}\text{Cr}_{21}\text{Ni}_{23}$  (filled diamonds) obtained at 800 K in the DLM-LSF calculations. Small filled circles show the results for  $\text{Fe}_{56}\text{Cr}_{21}\text{Ni}_{23}$  without LSF (which means DLM calculations for Fe and non-spin-polarized for Cr and Ni).

Ni and Fe-Cr pairs, which should be small anyway. As for the Ni-Cr strain-induced interactions, we take them from Ref. 34 where they have been obtained for Ni-Cr binary alloys. Although this is a quite rough approximation, it is used here to test a qualitative effect of such interactions onto the ordering in austenitic steels.

Multisite interactions are relatively small in these alloys. The strongest 3-site interaction is of the 114-type (for the nomenclature of the multisite interactions see Ref. 34), i.e. for the cluster of the three nearest-neighbors on the line in the closed packed [110] direction (there are 8 such interactions in general for a given 3-site cluster, which correspond to different combinations of alloy indexes). It is especially strong for the  $\text{CrCrCr}[\text{Ni}]$  configuration: 3.11 and 2.86 mRy in  $\text{Fe}_{75}\text{Cr}_{17}\text{Ni}_{08}$  and  $\text{Fe}_{56}\text{Cr}_{21}\text{Ni}_{23}$ , respectively. This specific interaction corresponds actually to the same type of interaction in Ni-Cr binary alloy where it is in fact also the strongest 3-site interaction,<sup>34</sup> although the value of the interaction is quite reduced in ternary Fe-Cr-Ni alloys compared to that in binary Ni-Cr alloys.

The strongest 4-site interactions are for the tetrahedron of the nearest neighbors and for the four near-

est neighbor sites along the closed packed [110] direction, which are also the strongest interactions in the Ni-Cr system.<sup>34</sup> In ternary alloys, however, the quasibinary Fe-Ni 4-site interactions ( $\text{FeFeFeFe}[\text{Ni}]$ ) are comparable with the corresponding quasibinary Ni-Cr interactions ( $\text{CrCrCrCr}[\text{Ni}]$ ), while the interactions with mixed alloy component indexes are almost an order of magnitude smaller.<sup>35</sup>

In order to check how the SGPM works, for this particular system, the ordering energy of the  $\text{Fe}_2\text{NiCr-L1}_2\text{m}$  ordered structure in the DLM state (without LSF) have been calculated for the lattice constant of 3.615 Å from the EMT total energies and from SGPM interactions for  $\text{Fe}_{50}\text{Ni}_{25}\text{Cr}_{25}$  random alloy. In the direct calculations the ordering energy is -1 mRy/atom, while it is about -2 mRy/atom from the pair, 3-site and 4-site SGPM interactions. The agreement is reasonable, considering the smallness of the ordering energy, and the fact that magnetic moment in the ordered state,  $1.0 \mu_B$ , is different from that in the random alloy,  $1.6 \mu_B$ . Such a small ordering energy (160 K) also means that this structure can hardly be formed at 650 K as predicted in Ref. 9.

One of the reasons why the ordering strength is greatly exaggerated in Ref. 9 is the fact that its authors are using concentration independent cluster expansion for 0 K enthalpies of formation obtained in the ferromagnetic state (with ferromagnetic alignment of Fe and Ni magnetic moments and antiferromagnetic one of Cr and Fe(Ni)) in the high temperature Monte Carlo simulations. To show the effect of the magnetic state upon the effective interactions, we compare in Fig. 6 the effective pair interactions for random  $\text{Fe}_{56}\text{Cr}_{21}\text{Ni}_{23}$  alloy obtained in the DLM-LSF state at 800 K and in the ferromagnetic (FM) state (again, the magnetic moment of Cr is antiferromagnetically aligned with those of Fe and Ni).

Although the Ni-Cr effective pair interactions are approximately the same in both states, it is obviously not the case of the Fe-Cr and Fe-Ni effective pair interactions: the strongest nearest neighbor interaction for both pairs is more than twice as large in the FM state as in the DLM-LSF state. Such a strong dependence of the effective interactions on the magnetic state means that the corresponding modeling of austenitic steels at finite temperatures should be done in the relevant to this temperature magnetic state.

Let us note that the effect of the magnetic state upon chemical interactions in fcc Fe-Ni alloys have been already studied in Ref. 36 and 37. In particular, as has been demonstrated in Ref. 36, the DLM state leads to a significant drop of the strongest nearest neighbor interaction in Invar  $\text{Fe}_{65}\text{Ni}_{35}$  alloy, which makes, in the end, the ordering of this alloy impossible at temperatures relevant to its preparation. It is interesting that the interactions obtained in Ref. 36 for the Invar binary alloy are very close to those for  $\text{Fe}_{56}\text{Cr}_{21}\text{Ni}_{23}$  shown in Fig. 6.

It has been also demonstrated<sup>37</sup> that there is a substantial reduction of the effective chemical interactions even in the finite temperature FM state due to a reduce



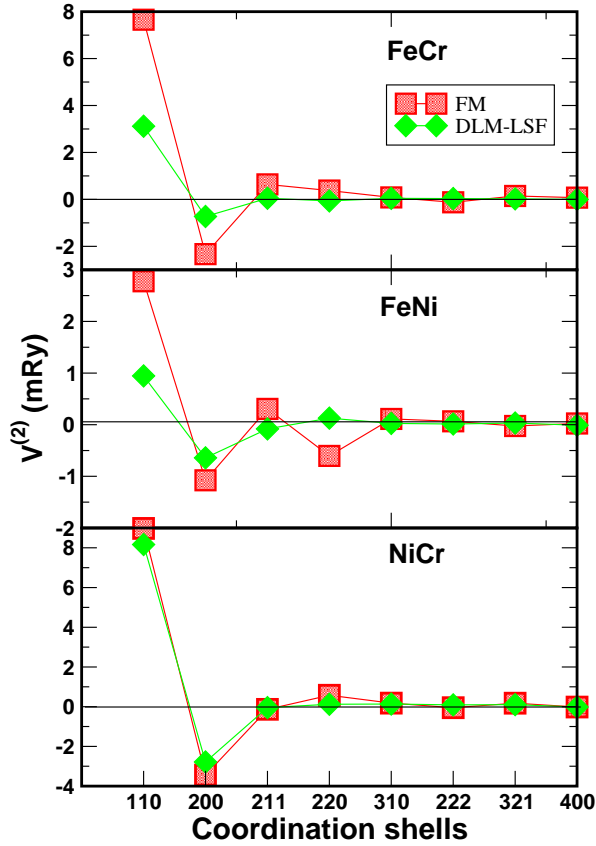


FIG. 6. (Color online) Effective pair interactions in  $\text{Fe}_{56}\text{Cr}_{21}\text{Ni}_{23}$  obtained in the DLM-LSF state at 800 K and in the ferromagnetic (FM) state.

magnetization, which is very similar to the case of bcc Fe-Cr alloys.<sup>38</sup> It is obvious that such a coupling between magnetic state and effective interactions should be properly taken into consideration in the corresponding thermodynamic modeling at high temperatures.

## VI. ATOMIC ORDERING IN AUSTENITIC STEELS

Monte Carlo calculations of atomic alloy configuration in  $\text{Fe}_{75}\text{Cr}_{17}\text{Ni}_{08}$  and  $\text{Fe}_{56}\text{Cr}_{21}\text{Ni}_{23}$  alloys have been done using a simulation box containing  $12 \times 12 \times 12 (\times 4)$  sites. In both cases, the first 21 effective pair interactions have been used with the contribution from the Ni-Cr strain-induced interactions taken from Ref. 34. We have also used the four strongest 3-site interactions of the 111, 112, 113 and 114-type (see Ref. 34 for the nomenclature), and two 4-site interactions, for the tetrahedron of the nearest neighbors and the nearest neighbor sites along the closed packed [110] direction.

The calculated atomic SRO parameters at 800 K are presented in Table I together with the experimental data from Ref. 7. Although the agreement is only qualitative, one should take into consideration the fact that the

strain-induced interactions are considered only quite approximately in this work. Besides, the experimental values seem to be quite sensitive to the model used in the analysis of the diffuse scattering intensities.

Nevertheless, the picture of atomic ordering is quite clear and consistent: the strongest ordering is between Ni and Cr nearest and next nearest neighbors. The calculated type of ordering is (100), which is the same as in the experiment, but it is different from the  $(1\frac{1}{2}0)$  type in the ordered  $\text{Ni}_2\text{Cr}$  phase. However, as has been shown in Ref. 34, the effective cluster interactions and ordering are sensitive to the alloy composition in fcc Ni-Cr alloys, and the (100)-type ordering is consistent with the results for equiatomic Ni-Cr alloys.

The next in the strength of ordering are the pairs of Fe and Cr atoms at the first coordination shell. Although the type of ordering in theoretical calculations, (100) is not consistent with the experimental one,  $(1\frac{1}{2}0)$ , one can again notice that the type of ordering in the experiment depends on the fitting model.<sup>7</sup> We have also neglected the Fe-Cr strain-induced interactions, which may produce a certain effect.

And finally, Fe and Ni atoms repel each other at the first coordination shell exhibiting there a kind of "phase separation" behavior, although the corresponding effective pair interaction is of an ordering type. As has been already mentioned, the Fe-Ni effective pair interactions in binary Invar alloy,  $\text{Fe}_{65}\text{Ni}_{35}$ ,<sup>36</sup> are very close to those obtained in this work for austenite and shown in Fig. 5, where the slight ordering tendency is observed. The difference between the atomic ordering of Fe and Ni atoms in Invar alloy and ternary  $\text{Fe}_{56}\text{Cr}_{21}\text{Ni}_{23}$  alloy is thus entirely due to compositional restrictions in the latter case, which do not allow atoms of all the types to establish their best local environment.

TABLE I. Warren-Cowley short-range-order parameters,  $\alpha_{lmn}^{\alpha\beta}$ , determined in Monte Carlo simulations for  $\text{Fe}_{56}\text{Cr}_{21}\text{Ni}_{23}$  Ni at 800 K. The experimental parameters are taken from Ref. 7.

| $lmn$ | $\alpha_{lmn}^{\text{FeCr}}$ |        | $\alpha_{lmn}^{\text{FeNi}}$ |        | $\alpha_{lmn}^{\text{NiCr}}$ |        |
|-------|------------------------------|--------|------------------------------|--------|------------------------------|--------|
|       | Exp.                         | Calc.  | Exp.                         | Calc.  | Exp.                         | Calc.  |
| 110   | -0.009                       | -0.029 | 0.017                        | 0.032  | -0.113                       | -0.235 |
| 200   | 0.043                        | 0.032  | -0.002                       | -0.012 | 0.148                        | 0.261  |
| 211   | 0.029                        | 0.003  | -0.002                       | 0.013  | 0.012                        | -0.023 |
| 220   | -0.017                       | 0.021  | 0.001                        | -0.013 | 0.007                        | 0.060  |
| 310   | -0.024                       | -0.007 | 0.003                        | 0.004  | -0.003                       | -0.033 |
| 222   | -0.033                       | 0.006  | 0.003                        | -0.004 | 0.012                        | 0.021  |
| 321   | 0.005                        | -0.004 | 0.002                        | -0.001 | -0.004                       | -0.003 |
| 400   | -0.029                       | 0.008  | -0.002                       | -0.001 | 0.026                        | 0.019  |

It should be noted that the experimental data for the SRO parameters in  $\text{Fe}_{82-x}\text{Cr}_{18}\text{Ni}_x$  ( $x = 15, 20$ , and 25 wt.%) alloys obtained by Braude *et al.*<sup>8</sup> for temperatures 1400 K, seem to be quite strange. For instance, the Warren-Cowley SRO parameter for Ni-Cr pairs is about

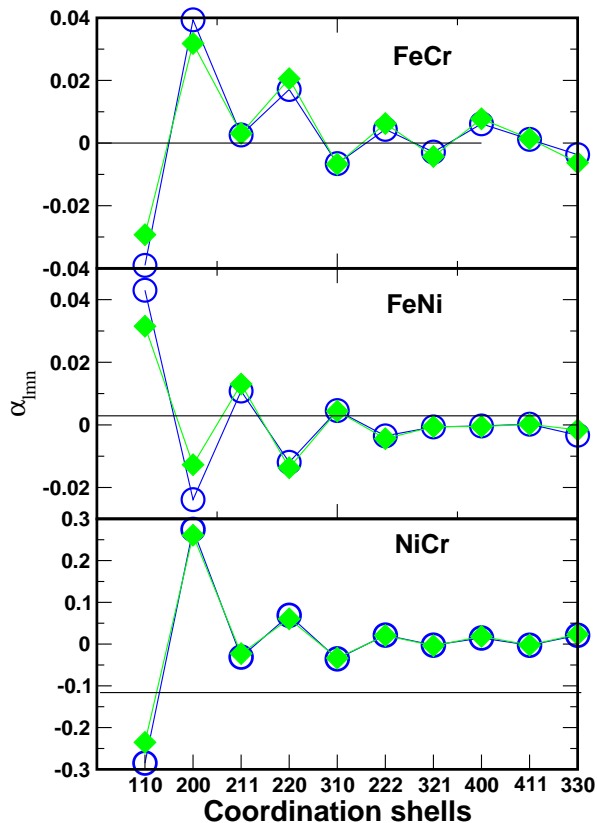


FIG. 7. (Color online) Warren-Cowley short-range order parameters in  $\text{Fe}_{75}\text{Cr}_{17}\text{Ni}_{08}$  (open circles) and  $\text{Fe}_{56}\text{Cr}_{21}\text{Ni}_{23}$  (filled diamonds) at 800 K obtained in Monte Carlo simulations.

−0.3 for the first (110) and second (200) coordination shells, while it is about 0.15 for the fourth (220) coordination shell. It is hard to imagine that kind of ordering behavior and it also contradicts experimental data by Cenedese *et al.*<sup>7</sup> The only common point is the fact that the ordering tendency between pairs of alloy components decreases in the order: Ni-Cr, Fe-Cr, and Fe-Ni.

The closeness of effective interactions and compositions for  $\text{Fe}_{56}\text{Cr}_{21}\text{Ni}_{23}$  and  $\text{Fe}_{75}\text{Cr}_{17}\text{Ni}_{08}$  alloys means that the atomic SRO should be also very similar. In Fig. 7, we show the atomic SRO in these alloys at 800 K. One can see that this is indeed the case: there is quite strong ordering of Ni-Cr atoms. In both cases the values of the SRO parameters are quite large (in absolute value), which means that these alloys should not be that far from an order-disorder phase transition.

Indeed, upon decreasing temperature the phase transition into the  $(\text{Fe,Ni})_3\text{Cr-L1}_2$ -like structure is observed at about 520 K for the  $\text{Fe}_{56}\text{Cr}_{21}\text{Ni}_{23}$  alloy composition and at 480 K for the  $\text{Fe}_{75}\text{Cr}_{17}\text{Ni}_{08}$  alloy composition, although most probably these transition temperatures are overestimated since the theoretical atomic SRO is stronger than experimental one. The ordered structure is shown in Fig. 8 for the case of  $\text{Fe}_{56}\text{Cr}_{21}\text{Ni}_{23}$  alloy (a similar structure is observed in the Monte Carlo simula-

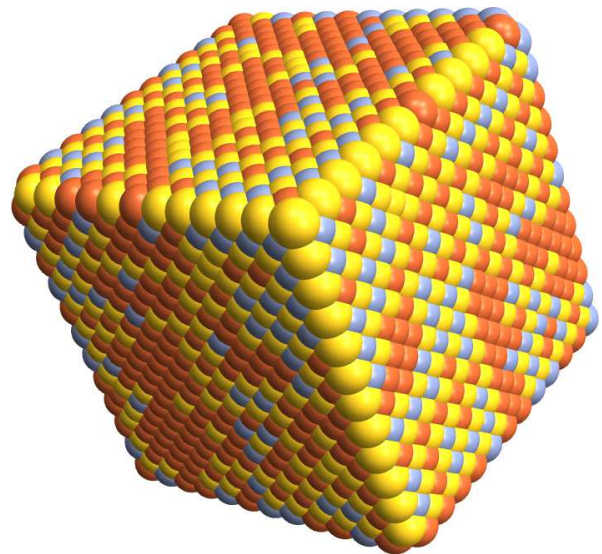


FIG. 8. (Color online) Atomic structure of  $\text{Fe}_{56}\text{Cr}_{21}\text{Ni}_{23}$  at 400 K obtained in Monte Carlo simulations. Type of atoms are colorcoded in the following way: Cr is yellow, Fe is red, and Ni is grayblue.

tions for  $\text{Fe}_{75}\text{Cr}_{17}\text{Ni}_{08}$ ).

As one can see, Cr atoms occupy a simple cubic positions of the fcc lattice, while Ni and Fe atoms occupy the remaining (face-centred) positions forming a peculiar mutual ordering. If the temperature in Monte Carlo simulations is lowered further, there will another phase transition at about 170 K leading to a mixture of two ordered phases:  $\text{Fe}_3\text{Ni}_3\text{Cr}_2$  and some not so clear ordering pattern of the remaining Fe and Cr atoms. However, this last transition is hardly relevant to the reality, where low temperature magnetic state can change substantially the interactions, and the atomic diffusion is absent on the usual practical human time scale.

## VII. SUMMARY

An accurate *ab initio*-based description of the finite-temperature properties of austenitic stainless steels require taking the thermally induced LSF into consideration. In this work, the simplest model has been used, which is based on a classical consideration of the spin-fluctuation energy, which is a rough statical single-site mean-field approximation. It is demonstrated, however, that it allows one to bring such properties as bulk modulus in close agreement with experimental data.

The simulations of atomic configuration of austenitic steels done for two compositions,  $\text{Fe}_{56}\text{Cr}_{21}\text{Ni}_{23}$  and  $\text{Fe}_{75}\text{Cr}_{17}\text{Ni}_{08}$ , show that there is substantial degree of the atomic SRO at high temperatures. These results are in reasonable agreement with the existing experimental data.<sup>7</sup> The theoretical calculations by Wrobel *et al.*<sup>9</sup> predict much stronger ordering tendency due to the use of



the low-temperature magnetic ground state in the cluster expansion. In this paper, we show that Fe-Cr and Fe-Ni effective pair interactions at the first coordination shell are approximately twice as large as those in the DLM(-LSF) state.

In order to establish a truly quantitative picture of the atomic ordering and the properties of austenitic steels at finite temperature, further investigation is needed into the finite temperature magnetism of these alloys and its use in the atomistic scale modeling of their structural and vibrational properties.

### Appendix A: SGPM interactions in the EMTO-CPA method

The one-electron contribution to the GPM interactions within the EMTO-CPA Green's function formalism can be obtained from the one-electron energy, which in this case is (for details of the EMTO-CPA parameters see<sup>11</sup>)

$$E_{one-el} = \frac{1}{2\pi i} \oint z \langle G(z) \rangle dz, \quad (A1)$$

where  $\langle G(z) \rangle$  is the CPA average Green's function of alloy (for Bravais lattice to simplify notations):

$$\langle G(z) \rangle = \int_{\text{BZ}} d\mathbf{k} \sum_{LL'} \tilde{g}_{L';L}(\mathbf{k}, z) \dot{S}_{L;L'}(\mathbf{k}, z) + s.s.c. \quad (A2)$$

Here, only multisite term is explicitly shown, while single-site contribution (s.s.c) is omitted since it does not contribute to the intersite chemical and magnetic interactions. Summations are running over sublattices ( $ij$ ), indexes of angular momentum ( $L, L'$ ) and integration is done over  $\mathbf{k}$ -points of the Brillouin zone.  $\dot{S}_{LL'}(\mathbf{k}, z)$  is the energy derivative of the slope matrix,  $S_{LL'}(\mathbf{k}, z)$ , which depend on energy,  $z$ , and  $\mathbf{k}$ -point, and  $\tilde{g}_{LL'}(\mathbf{k}, z)$  is the  $\mathbf{k}$ -point resolved CPA path operator:

$$\tilde{g}_{LL'}(\mathbf{k}, z) = \frac{1}{S_{LL'}(\mathbf{k}, z) - \tilde{D}_L(z)}, \quad (A3)$$

where  $\tilde{D}_L(z)$  is the coherent potential function of the EMTO method obtained self-consistently from the following CPA set of equations:

$$\tilde{g}_{LL'}(z) = \int d\mathbf{k} \tilde{g}_{LL'}(\mathbf{k}, z) \equiv \tilde{g} \quad (A4)$$

$$g^\alpha = \tilde{g} + \tilde{g} [D^\alpha - \tilde{D}] g^\alpha \quad (A5)$$

$$\tilde{g} = \sum_{\alpha} c^\alpha g^\alpha \quad (A6)$$

In the last two equations, we have omitted angular momentum index and energy dependence of  $\tilde{g}$  and  $D$ .

The chemical and magnetic exchange interactions then can be found using the force theorem<sup>39</sup> either for chemical fluctuations at some particular site (relative to the CPA effective medium)<sup>18,20,40-43</sup> or by introducing small displacement of the direction of the spin relative to unperturbed spin orientation at this site<sup>44-46</sup> and then finding the change of the one-electron energy (A1) by expanding the multisite part of the Green's function in (A2).

The resulting expressions are similar to those in the KKR or KKR-ASA methods.<sup>20</sup> For instance, the GPM quasibinary effective pair interactions in a multicomponent alloy are

$$\tilde{V}_p^{(2)-\alpha\beta-1} = -\frac{1}{\pi} \Im \int^{E_F} \text{Tr} [\Delta t^{\alpha\beta} \tilde{g}_{ij} \Delta t^{\alpha\beta} \tilde{g}_{ji}] dE, \quad (A7)$$

where  $\Delta t^{\alpha\beta} = t^\alpha - t^\beta$ , and  $t^\alpha$  has the meaning of the single-site scattering  $t$ -matrixes, which in the EMTO method are

$$t^\alpha = [1 + \tilde{g}(\tilde{D} - D^\alpha)]^{-1} (\tilde{D} - D^\alpha), \quad (A8)$$

which actually satisfy the CPA equation:

$$\sum_{\alpha} c^\alpha t^\alpha = 0. \quad (A9)$$

Another quantity entering (A7) is the CPA scattering path operator between  $i$  and  $j$  sites, which belong to the coordination shell  $p$ :

$$\tilde{g}_{ji}(z) = \int_{\text{BZ}} d\mathbf{k} \tilde{g}(\mathbf{k}, z) e^{i\mathbf{k}(\mathbf{R}_i - \mathbf{R}_j)} d\mathbf{k}, \quad (A10)$$

where angular momentum indexes are omitted.

In general, the interaction of order  $n$  of Hamiltonian (7) is defined as

$$V_f^{(n)-\alpha\beta\ldots\gamma[\delta]} = -\frac{1}{\pi} \Im \int^{E_F} \text{Tr} [t^\alpha \tilde{g}_{ij} t^\beta \tilde{g}_{jk} \ldots \tilde{g}_{lk} t^\gamma] dE, \quad (A11)$$

where  $i, j, \ldots$ , and  $k$  are the sites of the cluster  $f$ . As a matter of fact, this is only one specific contribution to this interaction, and in order to get the total interaction for  $n > 3$ , one should sum over all possible paths connecting sites of the cluster.

This formalism can be easily generalized to the case of paramagnetic alloys described by the DLM, or alloys with partial non-zero magnetization within partial DLM (PDLM) approach. In this case, the expressions for the effective interactions remain the same, but  $t^\alpha$  entering the corresponding formulas are modified. In particular, if alloy component A is in the PDLM state with magnetization  $m < 1$ , it is presented as an alloy with spin-up and spin-down orientation,  $A_x^\uparrow A_{1-x}^\downarrow$ , where

$m = 2x - 1$  (assuming that  $x \geq 0.5$ , and  $x = 0.5$  corresponds to the DLM paramagnetic state). It can be shown that corresponding magnetic averaging (like it is done, for instance, in Ref. 20 and 47) results in this case in  $t^A = xt^{A^\uparrow} + (1-x)t^{A^\downarrow}$  for every spin component.

Finally, in order to get the screened pair effective interaction at the coordination shell  $p$ , one should add the corresponding screening contribution,  $V_p^{scr-\alpha\beta}$ , as it is defined in (3), so that

$$\tilde{V}_p^{(2)-\alpha\beta} = \tilde{V}_p^{(2)-\alpha\beta-1} + V_p^{scr-\alpha\beta}. \quad (\text{A12})$$

## Appendix B: Magnetic exchange interactions in the EMTO-CPA method

Magnetic exchange interactions,  $J_p$  of Heisenberg Hamiltonian

$$H^H = - \sum_p \sum_{ij \in p} J_p \mathbf{e}_i \mathbf{e}_j, \quad (\text{B1})$$

where  $\mathbf{e}_i$  is the spin variable at site  $i$ , can be derived using the so-called magnetic force theorem<sup>45,46</sup> and has the following form for elementary solid closely resembling Eq. (A7):

$$J_p = -\frac{1}{\pi} \Im \int^{E_F} \text{Tr} [\Delta g_{ij}^\uparrow \Delta g_{ji}^\downarrow] dE, \quad (\text{B2})$$

where  $\Delta = D^\uparrow - D^\downarrow$ , and  $g_{ij}^{\uparrow(\downarrow)}$  are the intersite path operator for spin-up (and spin-down) states as they determined in (A10).

In the case of a random alloy, magnetic exchange interactions between  $\alpha$  and  $\beta$  alloy components,  $J_p^{\alpha\beta}$ , is determined as<sup>46</sup>

$$J_p^{\alpha\beta} = -\frac{1}{\pi} \Im \int^{E_F} \text{Tr} [\Delta^\alpha \bar{g}_{ij}^{\alpha\beta\uparrow} \Delta^\beta \bar{g}_{ji}^{\beta\alpha\downarrow}] dE, \quad (\text{B3})$$

where  $\Delta^\alpha = D^{\alpha\uparrow} - D^{\alpha\downarrow}$  and

$$\bar{g}_{ij}^{\alpha\beta} = [1 + \tilde{g}(\tilde{D} - D^\alpha)]^{-1} \tilde{g}_{ij} [1 + (\tilde{D} - D^\beta)\tilde{g}]^{-1}. \quad (\text{B4})$$

Here, it is assumed that alloy is homogeneous and thus there is no site-dependence of the potential parameters (although the generalization to inhomogeneous alloys is straightforward).

The DLM state is a special one since magnetic exchange interactions in the DLM state are equal to the corresponding GPM interactions  $8J_p = -\tilde{V}_p^{(2)}$ ,<sup>46,48</sup> which can be proved analytically. On the other hand, it follows from the comparison of the Ising and Heisenberg Hamiltonians and the fact that the last one is reduced to the Ising one for collinear magnetic configurations. This also means that GPM provides an easy way to calculated higher order magnetic interactions.<sup>20,48</sup>

## ACKNOWLEDGMENTS

AVR acknowledges the support of the Swedish Research Council (VR project 2015-05538), the European Research Council grant, the VINNEX center Hero-m, financed by the Swedish Governmental Agency for Innovation Systems (VINNOVA), Swedish industry, and the Royal Institute of Technology (KTH). Calculations have been done using NSC (Linköping) and PDC (Stockholm) resources provided by the Swedish National Infrastructure for Computing (SNIC). The support by the Austrian Federal Government (in particular from Bundesministerium fr Verkehr, Innovation und Technologie and Bundesministerium fr Wirtschaft, Familie und Jugend) represented by sterreichische Forschungsfrderungsgesellschaft mbH and the Styrian and the Tyrolean Provincial Government, represented by Steirische Wirtschaftsforderungsgesellschaft mbH and Standortagentur Tirol, within the framework of the COMET Funding Programme is also gratefully acknowledged.

<sup>1</sup> A. K. Majumdar and P. V. Blanckenhagen, Phys. Rev. B **29** 4079 (1984).

<sup>2</sup> A. I. Lichtenstein and M. I. Katsnelson, and G. Kotliar, Phys. Rev. Lett. **87**, 067205 (2001); I. Leonov, A. I. Poteryaev, V. I. Anisimov, and D. Vollhardt, Phys. Rev. Lett. **106**, 106405 (2011).

<sup>3</sup> A. V. Ruban, S. Khmelevskiy, P. Mohn, and B. Johansson, Phys. Rev. B **75**, 054402 (2007).

<sup>4</sup> A. V. Ruban, A. B. Belonoshko, and N. V. Skorodumova, Phys. Rev. B **87**, 014405 (2013).

<sup>5</sup> T. Moriya, and Y. Takahashi, J. of Phys. Soc. Jap. **45**, 397 (1978); J. Phys. (Paris) **39**, C6-1466 (1978).

<sup>6</sup> T. Moriya, *Spin Fluctuations in Itinerant Electron Magnetism* (Springer, Berlin, 1985).

<sup>7</sup> P. Cenedese, F. Bley, and S. Lefebvre, Acta Cryst. **A 40**, 228 (1984).

<sup>8</sup> I. S. Braude, V. I. Pechaerskaya, D. N. Bolshutkin, and M. M. Chernik, Cryst. Res. Technol. **21**, 253 (1986).

<sup>9</sup> J. S. Wrobel, D. Nguyen-Manh, M. Yu. Lavrentiev, M. Muzyk, and S. L. Dudarev, Phys. Rev. B **91**, 024108

- (2015).
- <sup>10</sup> O. K. Andersen, O. Jepsen, and G. Krier: In V. Kumar, O. K. Andersen, and A. Mookerjee (eds.) *Lectures on Methods of Electronic Structure Calculations* (World Scientific Publishing Co., Singapore, 1994), p. 63.
  - <sup>11</sup> L. Vitos, *Computational Quantum Mechanics for Materials Engineers* (Springer-Verlag, London, 2007).
  - <sup>12</sup> P. Soven, Phys. Rev. B **156**, 809 (1967); B. L. Gyorffy, Phys. Rev. B **5**, 2382 (1972).
  - <sup>13</sup> I. A. Abrikosov, A. M. N. Niklasson, S. I. Simak, B. Johansson, A. V. Ruban, and H. L. Skriver, Phys. Rev. Lett., **76** 4203 (1996); I. A. Abrikosov, S. I. Simak, B. Johansson, A. V. Ruban, and H. L. Skriver, Phys. Rev. B **56**, 9319 (1997).
  - <sup>14</sup> L. Vitos, I. A. Abrikosov, and B. Johansson, Phys. Rev. Lett. **87**, 156401 (2001).
  - <sup>15</sup> O.E. Peil, A.V. Ruban, and B. Johansson, Phys. Rev. B **85**, 165140 (2012).
  - <sup>16</sup> The Lyngby version of the EMT0 code properly takes into consideration electrostatics in random alloys in contrast to other existing versions. It is distributed by the author of the paper.
  - <sup>17</sup> A. V. Ruban and H. L. Skriver, Phys. Rev. B **66**, 024201 (2002); A. V. Ruban, S. I. Simak, P. A. Korzhavyi, and H. L. Skriver, *ibid*, 024202 (2002).
  - <sup>18</sup> F. Ducastelle and F. Gautier, J. Phys. F **6**, 2039 (1976).
  - <sup>19</sup> F. Ducastelle, *Order and Phase Stability in Alloys* (North-Holland, 1991).
  - <sup>20</sup> A. V. Ruban, S. Shallcross, S. I. Simak, and H. L. Skriver, Phys. Rev. B **70**, 125115 (2004).
  - <sup>21</sup> J. P. Perdew and Y. Wang, Phys. Rev. B **45**, 13244 (1992).
  - <sup>22</sup> J. P. Perdew, K. Burke, and M. Ernzerhof, Phys. Rev. Lett., **77**, 3865 (1996).
  - <sup>23</sup> H. J. Monkhorst and J. D. Pack, Phys. Rev. B **13**, 5188 (1972).
  - <sup>24</sup> M. Cyrot, Phys. Rev. Lett. **25**, 871 (1970); J. Phys. (Paris) **33**, 125 (1972).
  - <sup>25</sup> B. L. Gyorffy, A. J. Pindor, J. B. Staunton, G. M. Stocks, and H. Winter, J. Phys. F **15**, 1337 (1985).
  - <sup>26</sup> J. B. Staunton and B. L. Gyorffy Phys. Rev. Lett. **69**, 371 (1992).
  - <sup>27</sup> M. Uhl and J. Kubler, Phys. Rev. Lett. **77**, 334 (1996).
  - <sup>28</sup> N. M. Rosengaard and B. Johansson, Phys. Rev. B **55**, 14 975 (1997).
  - <sup>29</sup> J. Kübler, *Theory of Itinerant Electron Magnetism*, (Clarendon Press, Oxford, 2000), p. 323.
  - <sup>30</sup> N. D. Mermin, Phys. Rev. **137**, A1441 (1965).
  - <sup>31</sup> A. Teklu, H. Ledbetter, S. Kim, L. A. Boatner, M. McGuire, and V. Keppens, Metal. Mat. Trans. A **35**, 3149 (2004).
  - <sup>32</sup> A. V. Ruban and H. L. Skriver, Phys. Rev. B **55**, 856 (1997).
  - <sup>33</sup> In its turn, the quasibinary pair interactions are  $\tilde{V}_p^{(2)-\alpha\delta} = V_p^{(2)-\alpha\alpha[\delta]}$  and  $\tilde{V}_p^{(2)-\alpha\beta} = V_p^{(2)-\alpha\alpha[\delta]} + V_p^{(2)-\beta\beta[\delta]} - 2V_p^{(2)-\alpha\beta[\delta]}$ .
  - <sup>34</sup> M. Rahaman, B. Johansson, and A. V. Ruban, Phys. Rev. B **89**, 064103 (2014).
  - <sup>35</sup> For example, the 4-site interactions for the tetrahedron of the nearest neighbors are 1.54, -0.16, -0.09, -0.19, and 0.91 mRy for FeFeFeFe, CrFeFeFe, CrCrFeFe, CrCrCrFe, and CrCrCrCr alloy indexes, respectively.
  - <sup>36</sup> A. V. Ruban, S. Khmelevskyi, P. Mohn, and B. Johansson, Phys. Rev. B **76**, 014420 (2007).
  - <sup>37</sup> M. Ekholm, H. Zapolsky, A. V. Ruban, I. Vernyhora, D. Ledue, and I. A. Abrikosov, Phys. Rev. Lett. **105**, 167208 (2010).
  - <sup>38</sup> A. V. Ruban, P. A. Korzhavyi, and B. Johansson, Phys. Rev. B **77**, 094436 (2008).
  - <sup>39</sup> A. R. Mackintosh and O. K. Andersen, in *Electrons at the Fermi Surface*, edited by M. Springford (Cambridge University Press, Cambridge, England, 1980)??.
  - <sup>40</sup> A. Gonis, X.-G. Zhang, A. J. Freeman, P. Turchi, G. M. Stocks, and D. M. Nicholson, Phys. Rev. B **36**, 4630 (1987).
  - <sup>41</sup> P. E. A. Turchi, G. M. Stocks, W. H. Butler, D. M. Nicholson, and A. Gonis, Phys. Rev. B **37**, 5982 (1988).
  - <sup>42</sup> V. Drchal, J. Kudrnovsky, L. Udvardi, P. Weinberger, and A. Pasturel, Phys. Rev. B **45**, 14 328 (1992).
  - <sup>43</sup> P. P. Singh and A. Gonis, Phys. Rev. B **47**, 6744 (1993).
  - <sup>44</sup> T. Oguchi, K. Terakura, and H. Hamada, J. Phys. F: Met. Phys. **13**, 145 (1983); T. Oguchi, K. Terakura, and A. R. Williams, Phys. Rev. B **28**, 6443 (1983).
  - <sup>45</sup> A. Liechtenstein, M. I. Katsnelson, and V. A. Gubanov, J. Phys. F: Met. Phys. **14**, L125 (1984).
  - <sup>46</sup> A. Liechtenstein, M. I. Katsnelson, V. P. Antropov, and V. A. Gubanov, J. Magn. Magn. Mat. **67**, 65 (1987).
  - <sup>47</sup> M. Rahaman, A. V. Ruban, A. Mookerjee, and B. Johansson, Phys. Rev. B **83**, 054202 (2011).
  - <sup>48</sup> S. Shallcross, A. E. Kissavos, V. Meded, and A. V. Ruban, Phys. Rev. B **72**, 104437 (2005).